Proofs to Prof. M.A. Halcrow,

School of Chemistry, University of Leeds,

Woodhouse Lane, Leeds LS2 9JT, U.K.

Iron(II) Complexes of 2,6-Di(1-alkylpyrazol-3-yl)pyridine Derivatives – the Influence of Distal Substituents on the Spin State of the Iron Center

Thomas D. Roberts,[a] Marc A. Little,[a,b] Laurence J. Kershaw Cook,[a] Simon A. Barrett,[a]

Floriana Tuna[c] and Malcolm A. Halcrow*[,a]

[a]*School of Chemistry, University of Leeds,*

Woodhouse Lane, Leeds, LS2 9JT, U.K.

Fax: +44 113 343 6565

Email: M.A.Halcrow@leeds.ac.uk

[b]*Department of Chemistry, University of Liverpool*

Crown Street, Liverpool, UK L69 7ZD.

[c]*School of Chemistry and Photon Science Institute, University of Manchester,*

Oxford Road, Manchester, UK M13 9PL.

Dedicated to George Christou on the occasion of his 60th birthday.

TOC Entry

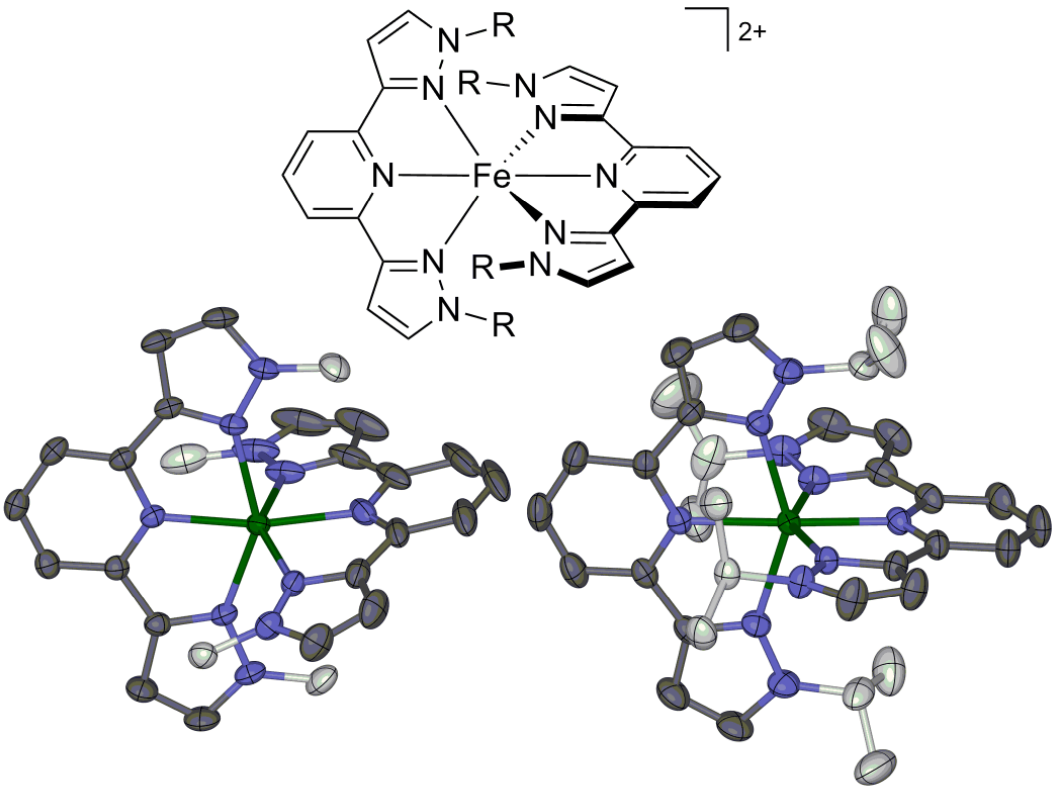

Four different complexes of the type shown, $[Fe(L^{R})_2]^{2+}$, have been prepared, with R = methyl, allyl, benzyl and *iso*propyl. All the compounds are high-spin in acetone solution and the solid state at room temperature and below, except for one salt of $[Fe(L^{Me})_2]^{2+}$ which is predominantly low-spin at 150 K in the crystal. This contrasts with the parent complex (R = H), which exhibits thermal spin-crossover just below room temperature.

Keywords

Iron; N-donor ligands; Crystal Structure; Magnetic Measurements; Spin-Crossover

ABSTRACT

2,6-Di(1-methyl-pyrazol-3-yl)pyridine (L^{Me}), 2,6-di(1-allyl-pyrazol-3-yl)pyridine (L^{All}), 2,6-di(1-benzyl-pyrazol-3-yl)pyridine (L^{Bz}) and di(1-*iso*propyl-pyrazol-3-yl)pyridine (L^{iPr}) have been synthesized by alkylation of deprotonated di{1*H*-pyrazol-3-yl}pyridine (3-bpp), and converted to salts of the corresponding $[Fe(L^{R})_2]^{2+}$ complexes (R = Me, All, Bz and *i*Pr). Crystal structures of $[Fe(L^{Me})_2]X_2$ ($X^- = BF_4^-$, ClO_4^- and PF_6^-), $[Fe(L^{All})_2][BF_4]_2$, $[Fe(L^{Bz})_2][BF_4]_2$ and $[Fe(L^{iPr})_2][PF_6]_2$ have been determined at 150 K. All of these contain high-spin iron centres except $[Fe(L^{Me})_2][BF_4]_2 \cdot xH_2O$, which is predominantly low-spin at that temperature. All the complexes are high-spin between 5-300 K as solvent-free bulk powders, and are also high-spin in $(CD_3)_2CO$ solution between 193-293 K. This was unexpected, since the parent complex $[Fe(3\text{-bpp})_2]^{2+}$ undergoes spin-crossover in the same solvent with $T_{½}$ = 247 K [Dalton Trans. 40 (2011) 12021]. The high-spin nature of the $[Fe(L^{R})_2]^{2+}$ complexes in solution must reflect a subtle balance of steric and electronic factors involving the ligand 'R' substituents.

INTRODUCTION

The chemistry of spin-crossover complexes [1-3] continues to be heavily studied, because of their potential applications as switchable components in memory and display devices [4], in nanoscience [2] and in MRI contrast agents [5]. A class of compound that has been heavily used in spin-crossover research during the past ten years are iron(II) complexes of the isomeric 2,6-di(pyrazolyl)pyridine ligands, 1-bpp and 3-bpp [6, 7]. The 1-bpp ligand framework can be substituted at every position of its pyrazole and pyridine rings [7]. Substitution at the pyridine ring allows functional groups to be included at the periphery of the $[Fe(1\text{-}bpp)_2]^{2+}$ centre without significantly perturbing the iron centre. This approach has afforded multifunctional spin-crossover complexes [8], coordination polymers of $[Fe(1\text{-}bpp)_2]^{2+}$ centres [9], and complexes with tether groups for deposition on surfaces [10]. In contrast, substituents at the pyrazole groups allow for steric and electronic control of the spin-state properties of a $[Fe(1\text{-}bpp)_2]^{2+}$ complex, so its spin-crossover properties can be modified in a rational way [7]. The synthetic versatility of $[Fe(1\text{-}bpp)_2]^{2+}$ is unique among the commonly used compounds in the field of spin-crossover.

<Insert Ligand Schematic here>

The coordination chemistry of substituted 3-bpp derivatives is less developed by comparison, because of the poorer availability of suitable synthetic precursors. However, 3-bpp ligands derivatised at *N*1 and *C*5 of the pyrazole rings are well-established, and have been employed in luminescent complexes [11-13], in catalysis [14-16], in hydrometallurgical applications [17] and in self-assembly reactions [18, 19]. However, although $[Fe(3\text{-}bpp)_2]^{2+}$ itself is a versatile spin-crossover compound [6], the application of substituted 3-bpp ligands to spin-crossover chemistry has only recently been investigated, by us [20] and by Aromí *et al* [21].

We describe here the first investigation of iron complexes of 3-bpp derivatives that are disubstituted at the pyrazole *N*1 positions. These are analogues of 1-bpp ligands bearing substituents at the pyrazole *C*3 sites, where the pyrazole substitutents are known to have a strong bearing on the spin-state properties of a coordinated iron centre [6]. Four 3-bpp derivatives have been investigated in this work: 2,6-di(1-methylpyrazol-3-yl)pyridine (L^{Me}), 2,6-di(1-allylpyrazol-3-yl)pyridine (L^{All}), 2,6-di(1-benzylpyrazol-3-yl)pyridine (L^{Bz}) and 2,6-di(1-*iso*propylpyrazol-3-yl)pyridine (L^{iPr}). Some noble metal complexes of L^{Me} [13] and L^{All} [16] have been reported before but their iron complexes have not yet been investigated, while L^{Bz} and L^{iPr} are new ligands to our knowledge. We were particularly interested in salts of $[Fe(L^{Me})_2]^{2+}$ since the $Fe[BF_4]_2$ complex of the equivalent 1-bpp derivative, 2,6-di(3-methylpyrazol-1-yl)pyridine (Me_2-1-bpp), exhibits an unusually low thermal spin-transition temperature for a complex of this type which leads to unique light-induced spin-crossover properties [22]. We were therefore keen to see whether salts of $[Fe(L^{Me})_2]^{2+}$ exhibit comparable effects.

EXPERIMENTAL

Unless otherwise stated, all manipulations were carried out in air using reagent-grade solvents. 2,6-Di(pyrazol-3-yl)pyridine (3-bpp) [23], 2,6-di(1-methylpyrazol-3-yl)pyridine (L^{Me}) [13] and 2,6-di(1-allylpyrazol-3-yl)pyridine (L^{All}) [16] were prepared by literature methods, while all other reagents and solvents were used as supplied.

Synthesis of 2,6-di(1-benzylpyrazol-3-yl)pyridine (L^{Bz})

2,6-*Bis*(pyrazol-3-yl)pyridine (2.00 g, 9.5 mmol) and lithium hydride (0.22 g, 28.4 mmol) were suspended in dry THF, in the presence of benzyl bromide (4.86 g, 28.4 mmol). The mixture was then heated at reflux for 44 hours under a nitrogen atmosphere. The resultant

white precipitate was removed via filtration and washed with water. The solid was then recrystallised from chloroform and dried *in vacuo*. Yield 1.67 g, 45 %. EI HR mass spectrum: *m*/*z* 391.1795 ($[L^{Bz}]^+$; calcd for $C_{25}H_{21}N_5$ *m*/*z* 391.1797). ^{1}H NMR ($CDCl_3$) δ 5.31 (br s, 4H, CH_2), 7.01 (br s, 2H, Pz H^4), 7.18-7.38 (br m, 10H, C_6H_5), 7.40 (d, 2.3 Hz, 2H, Pz $H^{5`}$), 7.75 (t, 7.5 Hz, 1H, Py H^4), 7.86 (br s, 2H, Py $H^{3/5}$). ^{13}C{^{1}H} NMR ($CDCl_3$): δ 56.2 (2C, CH$_2$), 105.2 (2C, Pz C^4), 118.6 (2C, Py $C^{3/5}$), 127.5 (Ph $C^{2/6}$), 128.0 (Ph $C^{3/5}$), 128.8 (Ph C^4), 130.9 (2C, Pz C^5), 136.4 (2C, Ph C^1), 137.3 (1C, Py C^4), 151.7 and 152.0 (both 2C, Py $C^{2/6}$ and Pz C^3).

Synthesis of 2,6-di(1-isopropylpyrazol-3-yl)pyridine (L^{iPr})

The same method as described for L^{Bz} was followed, using 2-iodopropane (4.83 g, 28.4 mmol). After 72 hrs at reflux under a nitrogen atmosphere, the resultant white precipitate was collected, washed with water and dried *in vacuo*. The product was employed without further purification. Yield 2.67 g, 95 %. EI HR mass spectrum: *m*/*z* 296.1874 ($[HL^{iPr}]^+$; calcd for $C_{17}H_{22}N_5$ *m*/*z* 296.1870). ^{1}H NMR ({CD_3}SO) δ 1.47 (d, 6.6 Hz, 12H, CH{CH_3}$_2$), 4.57 (sept, 6.6 Hz, 2H, CH{CH_3}$_2$), 6.92 (d, 2.1 Hz, 2H, Pz H^4), 7.83 (s, 2H, Pz H^5), 7.84 (s, 3H, Py $H^{3\text{-}5}$). ^{13}C{^{1}H} NMR ({CD_3}SO): δ 22.2 (4C, CH{CH$_3$}$_2$), 54.3 (2C, CH{CH_3}$_2$), 104.0 (2C, Pz C^4), 119.3 (2C, Py $C^{3/5}$), 128.9 (2C, Pz C^5), 139.0 (1C, Py C^4), 149.6 and 151.0 (both 2C, Py $C^{2/6}$ and Pz C^3).

Synthesis of the complexes

The same basic method, as described here for **1[BF$_4$]$_2$**, was followed for all the complexes in this study. Iron(II) tetrafluoroborate hexahydrate (0.14 g, 0.4 mmol) was added to a stirred solution of L^{Me} (0.20 g, 0.8 mmol) in nitromethane (15mL) and the resulting yellow solution was stirred for a further 30 minutes. Diethyl ether was then added until a yellow precipitate formed which was collected via filtration. The product was then recrystallised from

methanol/diethyl ether to give a yellow crystalline solid. The same method, using the equivalent quantities of the appropriate ligand and metal salt, yielded the other complexes. Recrystallised yields ranged from 38-70 %. **CAUTION** Although we have experienced no problems with **1[ClO$_4$]$_2$**, metal-organic perchlorates are potentially explosive and should be handled with due care in small quanitities.

Analytical data:

For [Fe(L^{Me})$_2$][BF$_4$]$_2$ (**1[BF$_4$]$_2$**): Found C, 44.0; H, 3.65; N, 19.7 %. Calcd. for $C_{26}H_{26}B_2F_8FeN_{10}$ C, 44.1; H, 3.70; N, 19.8 %. Electrospray mass spectrum: *m*/*z* 267.1 ([Fe(L^{Me})$_2$]$^{2+}$). ^{1}H NMR (CD$_3$OD): δ 2.2 (12H, C*H*$_3$), 22.6 (2H, Py *H*^{4}), 48.5 (4H, Pz *H*^{4}), 57.1 and 62.0 (both 4H, Py *H*$^{3/5}$ and Pz *H*^{5}).

For [Fe(L^{Me})$_2$][ClO$_4$]$_2$ (**1[ClO$_4$]$_2$**): Found C, 42.6; H, 3.50; N, 19.1 %. Calcd. for $C_{26}H_{26}C_{l2}FeN_{10}O_8$ C, 42.6; H, 3.57; N, 19.1 %. Electrospray mass spectrum: *m*/*z* 267.1 ([Fe(L^{Me})$_2$]$^{2+}$).

For [Fe(L^{Me})$_2$][PF$_6$]$_2$ (**1[PF$_6$]$_2$**): Found C, 37.8; H, 3.10; N, 17.1 %. Calcd. for $C_{26}H_{26}F_{12}FeN_{10}P_2$ C, 37.9; H, 3.18; N, 17.0 %. Electrospray mass spectrum: *m*/*z* 267.1 ([Fe(L^{Me})$_2$]$^{2+}$).

For [Fe(L^{All})$_2$][BF$_4$]$_2$ (**2[BF$_4$]$_2$**): Found C, 50.1; H, 4.15; N, 17.0 %. Calcd. for $C_{34}H_{34}B_2F_8FeN_{10}$ C, 50.3; H, 4.22; N, 17.2 %. Electrospray mass spectrum: *m*/*z* 319.12 ([Fe(L^{All})$_2$]$^{2+}$). ^{1}H NMR (CD$_3$CN): δ –0.6 (8H, C*H*$_2$), 2.1 (8H, CH=C*H*$_2$), 2.2 (4H, C*H*=CH$_2$), 21.7 (2H, Py *H*^{4}), 46.8 (4H, Pz *H*^{4}), 58.9 and 61.8 (both 4H, Py *H*$^{3/5}$ and Pz *H*^{5}).

For [Fe(L^{Bz})$_2$][BF$_4$]$_2$ (**3[BF$_4$]$_2$**): Found C, 58.8, H, 4.10; N, 13.8 %. Calcd. for $C_{50}H_{42}B_2F_8FeN_{10}$ C, 59.3; H, 4.18; N, 13.8 %. Electrospray mass spectrum: *m*/*z* 419.2 ([Fe(L^{Bz})$_2$]$^{2+}$). ^{1}H NMR (CD$_3$CN): δ –0.5 (8H, C*H*$_2$), 2.1 (8H, Ph *H*$^{2/6}$), 5.5 (8H, Ph *H*$^{3/5}$), 6.5 (4H, Ph *H*^{4}), 5.5 (8H, C*H*$_2$), 20.8 (2H, Py *H*^{4}), 46.0 (4H, Pz *H*^{4}), 59.5 and 60.9 (both 4H, Py *H*$^{3/5}$ and Pz *H*^{5}).

For $[Fe(L^{iPr})_2][BF_4]_2 \cdot H_2O$ (**4[BF$_4$]$_2$·H$_2$O**): Found C, 48.9; H, 4.95; N, 16.7 %. Calcd. for $C_{34}H_{42}B_2F_8FeN_{10} \cdot H_2O$ C, 48.7; H, 5.29; N, 16.7 %. Electrospray mass spectrum: *m*/*z* 323.2 ($[Fe(L^{iPr})_2]^{2+}$). ^{1}H NMR (CD_3CN): δ 2.0 and 2.1 (both 6H, CH{C*H*$_3$}$_2$), 4.7 (4H, C*H*{CH$_3$}$_2$), 21.1 (2H, Py *H*^{4}), 45.8 (4H, Pz *H*^{4}), 60.8 and 61.6 (both 4H, Py *H*$^{3/5}$ and Pz *H*^{5}).

For $[Fe(L^{iPr})_2][PF_6]_2$ (**4[PF$_6$]$_2$**): Found C, 43.2; H, 4.40; N, 14.9 %. Calcd. for $C_{34}H_{42}F_{12}FeN_{10}P_2$ C, 43.6; H, 4.52; N, 15.0 %. Electrospray mass spectrum: *m*/*z* 323.2 ($[Fe(L^{iPr})_2]^{2+}$).

Single crystal *X*-ray structure determinations

All the single crystals in this work were grown by slow diffusion of diethyl ether vapour into nitromethane or acetonitrile solutions of the compounds except for **1[BF$_4$]$_2$**·*x*H$_2$O which was crystallised from methanol/diethyl ether, and **2[BF$_4$]$_2$** which was crystallised from acetonitrile/di-*iso*propyl ether. Diffraction data were measured using a Bruker X8 Apex diffractometer fitted with an Oxford Cryostream low temperature device, using graphite-monochromated Mo-K_α radiation (λ = 0.71073 Å) generated by a rotating anode. Experimental details of the structure determinations in this study are given in Table 1. All the structures were solved by direct methods *(SHELXS97* [24]), and developed by full least-squares refinement on F^2 (*SHELXL97* [24]). Crystallographic figures were prepared using *XSEED* [25] which incorporates *POVRAY* [26].

<Insert Table 1 here>

***X*-ray structure determination of $[Fe(L^{Me})_2][BF_4]_2 \cdot xH_2O$ (1[BF$_4$]$_2$·*x*H$_2$O; *x* ≈ 1).** The asymmetric unit contains two half-molecules of the complex, labelled 'A' and 'B'. Fe(1A) spans the C_2 axis $^1/_2$, *y*, $^1/_4$, while Fe(1B), N(2B), C(5B), N(12B) and C(15B) lie on 0, *y*, $^1/_4$. There are also two unique anions and a disordered solvent site lying on general

crystallographic positions. Both anions are disordered over two sites, with independently refined occupancy ratios close to 0.6:0.4. The refined restraints B–F = 1.40(2) and F...F = 2.29(2) Å were applied to these residues. The disordered solvent site contained three Fourier peaks separated by 1.2 Å, that lie within hydrogen-bonding distance of one of the BF_4^- anion sites, and also with its own symmetry equivalent related by the crystallographic inversion centre *–x*, *–y*, 1*–z*. These were refined as three partial water sites, whose occupancies summed to 1. All non-H atoms with occupancy >0.5 were refined anisotropically, while C-bound H atoms were placed in calculated positions and refined using a riding model. The partial water H atoms could not be located and are not included in the model, but are accounted for in the density and *F*(000) calculations. The highest residual Fourier peak of +1.0 *e*. $Å^{-3}$ lies one of the disordered anions.

***X*-ray structure determination of $[Fe(L^{Me})_2][ClO_4]_2$ ($1[ClO_4]_2$).** The structure was originally solved in the monoclinic space group C_2, then transformed up to *R*32 following an initial refinement using the *ADSYMM* routine in *PLATON* [27]. The asymmetric unit contains: half a complex cation, with Fe(1) spanning the C_2 axis *x*, *x* + $^1/_3$, $^1/_6$; one-third of a ClO_4^- ion, with the Cl and one O atom lying on the C_3 axis 0, 0, *z*; half a ClO_4^- ion whose Cl atom spans the C_2 axis *x*, *x*, 0; and, one-sixth of a ClO_4^- ion disordered about the 32 site $^1/_3$, $^2/_3$, $^1/_6$, with the Cl atom lying on this position and one O atom on the axis $^1/_3$, $^2/_3$, *z*. The pyrazole ring C(14)-C(19) was modelled as disordered, over two equally occupied sites. The following restraints were applied to that residue: intra-ring C–C = 1.40(2), C–N = N–N = 1.34(2), N–C{methyl} = 1.48(2) and C–C{pyridyl} = 1.41(2) Å. Attempts to extend the disorder model to the complete complex half-cation did not afford a chemically reasonable refinement. No other disorder was included in the model, although some of the ClO_4^- O atoms also have slightly high displacement ellipsoids. All non-H atoms except for the

disordered ligand atoms were refined anisotropically, and H atoms were placed in calculated positions and refined using a riding model.

***X*-ray structure determinations of $[Fe(L^{Me})_2][PF_6]_2$ ($1[PF_6]_2$) and $[Fe(L^{Bz})_2][BF_4]_2$ ($3[BF_4]_2$).** The asymmetric units of these crystals contain one complete formula unit, with all the molecules lying on general crystallographic sites. No disorder was detected during the refinements, and no restraints were applied. All non-H atoms were refined anisotropically, and H atoms were placed in calculated positions and refined using a riding model.

***X*-ray structure determinations of $[Fe(L^{All})_2][BF_4]_2$ ($2[BF_4]_2$).** The asymmetric unit contains one-quarter of a complex dication, with Fe(1) lying on the $\bar{4}$ site $^3/_4$, $^7/_8$, $^1/_2$, and N(2) and C(5) on the C_2 axis $^3/_4$, *y*, $^1/_2$. There is also one-third of a crystallographically ordered BF_4^- ion, with B(14) and F(16) lying on the C_3 axis *x*, *x*, *x*; and, a second anion site with occupancy $^1/_6$ lying on a general crystallographic position close to the $\bar{4}$ site 1, $^3/_4$, $^5/_8$. The latter residue has very high displacement ellipsoids and is certainly disordered, although attempts to model this using two or three partial anion sites led to unstable refinements. It was therefore refined as a single site in the final least squares cycles, subject to the fixed restraints B–F = 1.35(2) and F...F = 2.20(2) Å. The unique allyl substituent is also disordered, and was refined over three orientations labelled 'A' (occupancy 0.60), 'B' (0.25) and 'C' (0.15). The fixed restraints C–N = 1.47(2), C–C = 1.51(2), C=C = 1.34(2), 1,3-C...N = 2.43(2) and 1,3-C...C = 2.46(2) Å were applied to this residue. All crystallographically ordered non-H atoms, plus the major allyl group disorder site, were refined anisotropically while H atoms were placed in calculated positions and refined using a riding model.

***X*-ray structure determination of $[Fe(L^{iPr})_2][PF_6]_2 \cdot 2MeCN$ ($4[PF_6]_2 \cdot 2MeCN$).** There are two formula units in the asymmetric unit (*Z*' = 2), whose complex cations are labelled 'A'

and ‘B’. Two of the four unique PF_6^- ions are disordered, one of them over three sites with a 0.4:0.4:0.2 occupancy ratio, and the other over two equally occupied orientations. The refined restraints P–F = 1.60(2) and *cis*-F...F = 2.61(2) Å were applied to those residues. One *iso*propyl group [C(13A)-C(15A)] was also disordered over two sites with refined occupancies of 0.8 and 0.2, and was modelled with the fixed restraints C–N = 1.48(2), C–C = 1.52(2), 1,3-C...N = 2.44(2) and 1,3-C...C = 2.48(2) Å. Finally one solvent molecule was modelled over two half-occupied sites, that were refined without restraints. All non-H atoms with occupancy ≥0.5 were refined anisotropically, except for the disordered solvent sites. All H atoms were placed in calculated positions and refined using a riding model.

Other measurements.

Electrospray mass spectra were obtained using a Waters Micromass ZQ4000 spectrometer from MeCN solution. CHN microanalyses were performed by the University of Leeds Department of Chemistry microanalytical service. Infra-red spectra were obtained as nujol mulls pressed between NaCl windows between 600-4,000 cm^{-1}, using a Nicolet Avatar 360 spectrophotometer. TGA measurements employed a TA Instruments TGA 2050 analyser. Magnetic susceptibility measurements were obtained using a Quantum Design SQUID magnetometer in an applied field of 1000 G. Diamagnetic corrections were estimated from Pascal’s constants [28], and a diamagnetic correction for the sample holder was also applied. Magnetochemical calculations and graph preparation were carried out using *SIGMAPLOT* [29]. Susceptibility measurements in solution were obtained by Evans method using a Bruker DRX500 spectrometer operating at 500.13 MHz [30]. A diamagnetic correction for the sample [28], and a correction for the variation of the density of the $(CD_3)_2CO$ solvent with temperature [31], were applied to these data.

RESULTS AND DISCUSSION

Alkylation of 3-bpp is achieved by deprotonating preformed 3-bpp with lithium hydride, and reacting the resultant dianion with appropriate alkyl halides [16, 32]. The desired *N*1,*N*1'-disubstituted products L^{Me} [13], L^{All} [16], L^{Bz} and L^{iPr} were cleanly obtained in each case, with no evidence for competitive alkylation at the pyrazole *N*2 sites [33]. This presumably reflects protection of the *N*2 sites of the doubly deprotonated $[3\text{-bpp}–2H]^{2–}$ intermediate by lithium ion chelation [34]. The salts $[Fe(L^{Me})_2]X_2$ (**1X₂**; $X^– = BF_4^–$, $ClO_4^–$ and $PF_6^–$) were prepared by treatment of the appropriate iron(II) salt with 2 equiv of L^{Me} in nitromethane at room temperature. Similar reactions with the other ligands afforded $[Fe(L^{All})_2][BF_4]_2$ (**2[BF₄]₂**) $[Fe(L^{Bz})_2][BF_4]_2$ (**3[BF₄]₂**) and $[Fe(L^{iPr})_2]Y_2$ (**4Y₂**, $Y^– = BF_4^–$ and $PF_6^–$; the $PF_6^–$ salt of this complex was also studied because it afforded better single crystals than the $BF_4^–$ salt).

Single crystal *X*-ray analyses at 150 K were obtained of all the complex salts in this work, except for **4[BF₄]₂** (Fig. 1, Tables 2 and 3). The crystallography of the compounds is quite varied, in that only **1[PF₆]₂** and **3[BF₄]₂** contain one complete formula unit with no internal symmetry in their asymmetric units. **1[BF₄]₂** crystallises as a monohydrate phase from undried MeOH/Et_2O, with two half-molecules of the complex spanning crystallographic C_2 axes. The asymmetric unit of **1[ClO₄]₂** contains one C_2-symmetric half-molecule, and is complicated by disorder in the unique L^{Me} ligand. This disorder is a consequence of a close intermolecular contact between one of the two unique pyrazole rings and its symmetry equivalent related by *–x*, *–x+y*, *–z*. Only the 'A' disorder site in one molecule of this pair, and the 'B' disorder site of the other, can be occupied at the same time, with a random distribution of 'A' and 'B' occupancies in each pair of half-cations throughout the crystal (Fig. 2). Crystalline **2[BF₄]₂** adopts a cubic space group with one-quarter of a formula unit in the asymmetric unit. The unique allyl substituent is extensively disordered, reflecting the

presence of a neighbouring BF_4^- anion site that is only part-occupied on charge neutrality grounds. Finally, the solvate **4[PF$_6$]$_2$**·2MeCN contains two formula units in its asymmetric unit (*i.e. Z*' = 2), with only minor structural differences between the two unique complex dications.

<Insert Figures 1 and 2, and Tables 2 and 3, here>

The iron centres in **1[PF$_6$]$_2$**, **2[BF$_4$]$_2$**, **3[BF$_4$]$_2$** and **4[PF$_6$]$_2$** are all clearly high-spin at this temperature (Tables 2 and 3), based on their Fe–N distances and the distortion parameters Σ and Θ (these measure the deviation of the FeN_6 polyhedron from an ideal octahedral geometry, which is always significantly larger in the high-spin state [35]). Consideration of **1[ClO$_4$]$_2$** is complicated by its ligand disorder (Fig. 2), but Σ and Θ imply that this complex is also high-spin at 150 K (Table 2). The only exception to this trend is **1[BF$_4$]$_2$**·*x*H_2O, whose asymmetric unit contains two unique half-molecules are predominantly low-spin at 150 K on the basis of their metric parameters. While molecule A is apparently fully low-spin, however, molecule B has a detectable residual high-spin fraction at that temperature according to its larger Fe–N bond lengths and distortion parameteres (Table 2). Interestingly, like **1[BF$_4$]$_2$**·*x*H_2O, [Fe(Me$_2$-1-bpp)$_2$][BF_4]$_2$ also crystallises as a hydrate phase from undried methanol, although the two compounds are not isostructural [22].

Comparison of the three **1X$_2$** salts (X^- = BF_4^-, ClO_4^- and PF_6^-) sheds some light on their different behaviour in the crystal (Fig. 3). The iron coordination geometry in **1[PF$_6$]$_2$** is unique in this study, in being significantly distorted from the ideal D_{2d} symmetry associated with a $[Fe(bpp)_2]^{2+}$ centre (Table 2). This angular distortion is is a manifestation of the Jahn-Teller effect in a high-spin d^6 ion [36-38], which is common in high-spin $[Fe(1\text{-bpp})_2]^{2+}$ derivatives but has rarely been seen thus far in their $[Fe(3\text{-bpp})_2]^{2+}$ analogues [7]. The distortion involves a reduction in the *trans*-N{pyridyl}–Fe–N{pyridyl} angle (ϕ) from its

ideal value of 180°, and/or a twisting of the two tridentate ligands away from the perpendicular (θ < 90º, where θ is the dihedral angle between the least squares planes of the two ligands). Distorted $[Fe(bpp)_2]^{2+}$ complexes in the solid phase are trapped in their high-spin state, since the structural changes required to convert them to their (undistorted) low-spin forms are too great to be accommodated by a rigid solid lattice. These angles in **1[PF$_6$]$_2$** imply a significant Jahn-Teller distortion is present in that salt, since they are significantly lower than their ideal values and lie in the range where spin-crossover would not normally be observed (Table 2) [7]. The Jahn-Teller distortion in **1[ClO$_4$]$_2$** is less clear cut because of the ligand disorder but is clearly smaller (Table 2), with a combination of distortion angles ϕ = 178.8° and $\theta \geq$ 83.3° that would not preclude spin-crossover based on our earlier work [7]. The twisted ligand conformation in that cation [38], and the close intermolecular contacts that give rise to the ligand disorder [39], are more likely to contribute to the inhibition of spin-crossover in that salt. In comparison, the fully and predominantly low-spin iron centres in **1[BF$_4$]$_2$**·xH$_2$O exhibit almost perfect D_{2d} molecular symmetry, with regular coordination geometries and essentially planar L^{Me} ligands (Fig. 3).

<Insert Figure 3 here>

Although some of the compounds contain occluded solvent in the crystalline state, after drying they all afford solvent-free bulk powders by elemental microanalysis except **4[BF$_4$]$_2$**, which analyses as a monohydrate. Variable temperature magnetic susceptibility measurements showed that bulk samples of all these solids are high-spin between 5-300 K (Fig. 4, top; the reduction in $\chi_M T$ below 50 K is not caused by spin-crossover, but reflects zero-field splitting of the high-spin iron centres [40]). In most cases that is consistent with their crystal structures, which contain high-spin iron centres at 150 K. The exception is **1[BF$_4$]$_2$**, which is almost fully low-spin in its hydrated crystal at 150 K but is high-spin as a solvent-free powder (the anhydrous nature of the sample was confirmed by a TGA analysis,

which showed <0.2 % mass loss below 500 K). Evidently, dehydration of crystalline **1[BF$_4$]$_2$**·*x*H$_2$O causes a structure change with a concomitant change in spin-state. Attempts to shed light on this by growing single crystals of solvent-free **1[BF$_4$]$_2$** have been unsuccessful, however.

<Insert Fig. 4 here>

Further insight into the spin-state properties of the complexes was gained from their solution behaviour, which was determined by variable temperature Evans method measurements in $(CD_3)_2CO$ [30]. The BF_4^- salts of all four complexes remain fully high-spin in this solvent, between 193-293 K (Fig. 4, bottom). This is unexpected, since the parent complex [Fe(3-bpp)$_2$][BF$_4$]$_2$ undergoes spin-crossover with a midpoint temperature $T_{½}$ = 247 K under the same conditions [41]. The methyl and *iso*propyl substituents in **1[BF$_4$]$_2$** and **4[BF$_4$]$_2$**·H$_2$O are electron-donating, which should stabilise the low-spin state of those complexes on inductive grounds, and thus raise $T_{½}$. Since this is not observed, the steric influence of the pyrazole substituents in **1[BF$_4$]$_2$**-**4[BF$_4$]$_2$**·H$_2$O must be more important in determining their spin-states. Notably the iron complex of the corresponding 1-bpp derivative, 2,6-di(3-*iso*propylpyrazol-1-yl)pyridine, is high-spin under the same conditions which was also attributed to the steric properties of the *iso*propyl groups in that compound [37, 42].

Space-filling plots of the crystal structures identify close intramolecular C–H…π interactions of 2.6-2.9 Å in **2[BF$_4$]$_2$**, **3[BF$_4$]$_2$** and **4[PF$_6$]$_2$** between the allyl, benzyl or *iso*propyl 'R' substituents of one L^R ligand and the pyridyl ring of the other (Fig. 5). Such close contacts will prevent spin-crossover on steric grounds, by inhibiting the associated contraction of the Fe–N bonds [42]. In $[Fe(L^{iPr})_2]^{2+}$ this steric repulsion is a consequence of the bulk of the *iso*propyl groups. The steric influence of the ligand substituents in $[Fe(L^{All})_2]^{2+}$ and $[Fe(L^{Bz})_2]^{2+}$ is less clear, but in both crystal structures there are individual allyl and benzyl

groups oriented to form comparably close inter-ligand contacts (Fig. 5). In the solid state the orientations of these substituents are fixed by the surrounding lattice, which would thus inhibit spin-crossover as observed. However the allyl group disorder in **2[BF$_4$]$_2$**, and the different benzyl conformations in **3[BF$_4$]$_2$**, imply that these substituents have a degree of conformational flexibility which would ameliorate these steric clashes during a spin-crossover equilibrium in solution. Moreover, there are no prohibitive intramolecular steric clashes involving the methyl groups in the salts of **1**$^{2+}$, while the predominantly low-spin nature of **1[BF$_4$]$_2$**·*x*H$_2$O at 150 K shows that [Fe(L^{Me})$_2$]$^{2+}$ can indeed undergo spin-crossover in principle (Fig. 5). Hence, the absence of spin-crossover in solution for **1[BF$_4$]$_2$**-**3[BF$_4$]$_2$** cannot be explained from steric effects alone, and must reflect a careful balance of steric and electronic influences.

<Insert Fig. 5 here>

CONCLUSION

Alkylation of the four pyrazolyl *N*1 sites in [Fe(3-bpp)$_2$]$^{2+}$ suppresses the thermal spin-crossover undergone by this complex, regardless of the steric and electronic properties of the new substitutents. Although the crystal structure of **1[BF$_4$]$_2$**·*x*H$_2$O shows that complex at least can undergo spin-crossover under certain conditions, all the other complex salts in this work remain high-spin at all the temperatures examined, in solution and the solid state. For **4X$_2$** (X$^-$ = BF$_4^-$ and PF$_6^-$) this was to be expected, owing to the steric influence of the L^{i}Pr *iso*propyl substituents [37, 42]. For the other complexes, whose ligand substituents are less bulky, the origin of their high-spin nature is less clear.

This result contrasts with the known chemistry of analogous complexes from the [Fe(1-bpp)$_2$]$^{2+}$ series [7]. Although solution phase data were not reported, some salts of [Fe(1-

bpp)$_2$]$^{2+}$ derivatives bearing methyl [22] or hydroxymethyl [43] substituents at the pyrazole *C*3 position do undergo thermal spin-crossover in the solid state. Moreover, the steric influence of the distal subsitutents in 1,1-disubstituted-3-bpp (L^R) and the corresponding 3,3-disubstituted-1-bpp ligands is essentially identical (Table 4). Hence it was unexpected that none of the complexes in this work should exhibit spin-crossover as bulk materials, or in solution. Conversely, however, for those compounds where a direct comparison is available, none of the complexes in this work is isostructural with its corresponding salt from the [Fe(1-bpp)$_2$]$^{2+}$ series [22, 37, 44]. Therefore, although the differences between [Fe(L^R)$_2$]$^{2+}$ and [Fe(1-bpp)$_2$]$^{2+}$ derivatives bearing the same distal 'R' substituents are small at the molecular level (Table 4 and Fig. 6), they are clearly sufficient to change their solid state chemistry.

<Insert Table 4 and Figure 6 here>

SUPPLEMENTARY DATA

CCDC 912782, 912783, 912784, 912785, 912786 and 912787 respectively contain the supplementary crystallographic data for **1[PF$_6$]$_2$**, **1[BF$_4$]$_2$**·*x*H$_2$O, **1[ClO$_4$]$_2$**, **4[PF$_6$]$_2$**·2CH$_3$CN, **3[BF$_4$]$_2$** and **2[BF$_4$]$_2$**. These data can be obtained free of charge via http://www.ccdc.cam.ac.uk/conts/retrieving.html, or from the Cambridge Crystallographic Data Centre, 12 Union Road, Cambridge CB2 1EZ, UK; fax: (+44) 1223-336-033; or e-mail: deposit@ccdc.cam.ac.uk.

ACKNOWLEDGEMENTS

This work was funded by the EPSRC.

REFERENCES

[1] M. A. Halcrow (ed.) Spin-crossover materials - properties and applications, John Wiley & Sons, Chichester, UK, p. 546 (2013).

[2] A. Bousseksou, G. Molnár, L. Salmon, W. Nicolazzi, Chem. Soc. Rev. 40 (2011) 3313.

[3] For other recent reviews see:

a) P. Gamez, J. S. Costa, M. Quesada, G. Aromí, Dalton Trans. (2009) 7845;

b) I. Šalitroš, N. T. Madhu, R. Boča, J. Pavlik, M. Ruben, Monatsh. Chem. 140 (2009) 695;

c) M. A. Halcrow, Chem. Soc. Rev. 40 (2011) 4119.

[4] O. Kahn, C. J. Martinez, Science 279 (1998) 44.

[5] J. Hasserodt, New J. Chem. 36 (2012) 1707.

[6] a) M. A. Halcrow, Coord. Chem. Rev. 249 (2005) 2880;

b) J. Olguín, S. Brooker, Coord. Chem. Rev. 255 (2011) 203.

[7] M. A. Halcrow, Coord. Chem. Rev. 253 (2009) 2493.

[8] a) M. Nihei, L. Han, H. Oshio, J. Am. Chem. Soc. 129 (2007) 5312;

b) M. Nihei, N. Takahashi, H. Nishikawa, H. Oshio, Dalton Trans. 40 (2011) 2154;

c) R. González-Prieto, B. Fleury, F. Schramm, G. Zoppellaro, R. Chandrasekar, O.Fuhr, S. Lebedkin, M. Kappes, M. Ruben, Dalton Trans. 40 (2011) 7564;

d) Y. Hasegawa, K. Takahashi, S. Kume, H. Nishihara, Chem. Commun. 47 (2011) 6846;

e) K. Takahashi, Y. Hasegawa, R. Sakamoto, M. Nishikawa, S. Kume, E. Nishibori, H. Nishihara, Inorg. Chem. 51 (2012) 5188.

[9] a) C. Rajadurai, O. Fuhr, R. Kruk, M. Ghafari, H. Hahn, M. Ruben, Chem. Commun. (2007) 2636;

b) J. Elhaïk, C. M. Pask, C. A. Kilner, M. A. Halcrow, Tetrahedron 63 (2007) 291.

[10] a) M. S. Alam, M. Stocker, K. Gieb, P. Müller, M. Haryono, K. Student, A. Grohmann, Angew. Chem. Int. Ed. 49 (2010) 1159;

b) V. Meded, A. Bagrets, K. Fink, R. Chandrasekar, M. Ruben, F. Evers, A. Bernand-Mantel, J. S. Seldenthuis, A. Beukman, H. S. J. van der Zant, Phys. Rev. B 83 (2011) 245415/1;

c) D. Secker, S. Wagner, S. Ballmann, R. Härtle, M. Thoss, H. B. Weber, Phys. Rev. Lett. 106 (2011) 136807/1.

[11] a) P. G. Potvin, P. U. Luyen, J. Brckow, J. Am. Chem. Soc. 125 (2003) 4894;

b) C.-C. Chou, K.-L. Wu, Y. Chi, W.-P. Hu, S. J.Yu, G.-H. Lee, C.-L. Lin, P.-T. Chou, Angew. Chem. Int. Ed. 50 (2011) 2054;

c) K.-L. Wu, C.-H. Li, Y. Chi, J. N. Clifford, L. Cabau, E. Palomares, Y.-M. Cheng, H.-A. Pan, P.-T. Chou, J. Am. Chem. Soc. 134 (2012) 7488.

[12] a) L. Zhao, K. M.-C. Wong, B. Li, W. Li, N. Zhu, L. Wu, V. W.-W. Yam, Chem. Eur. J. 16 (2010) 6797;

b) P. Wang, C.-H. Leung, D.-L. Ma, S.-C. Yan, C.-M. Che, Chem. Eur. J. 16 (2010) 6900.

[13] C.-M. Che, C.-F. Chow, M.-Y. Yuen, V. A. L. Roy, W. Lu, Y. Chen, S. S.-Y. Chui, N. Zhu, Chem. Sci. 2 (2011) 216.

[14] a) D. Zabel, A. Schubert, G. Wolmershäuser, R. L. Jones jr., W. R. Thiel, Eur. J. Inorg. Chem. (2008) 364;

b) L.-L. Miao, H.-X. Li, M. Yu, W. Zhao, W.-J. Gong, J. Gao, Z.-G. Ren, H.-F. Wang, J.-P. Lang, Dalton Trans. 41 (2012) 3424

[15] a) R. Jairam, M. L. Lau, J. Adorante, P. G. Potvin, J. Inorg. Biochem. 84 (2001) 113;

b) C. Kashima, S. Shibata, H. Yokoyama, T. Nishio, J. Heterocyclic Chem. 40 (2003) 773;

c) S. Günnaz, N. Özdemir, S. Dayan, O. Dayan, B. Çetinkaya, Organometallics 30 (2011) 4165;

d) L. Wang, H.-R. Pan, Q. Yang, H.-Y. Fu, H. Chen, R.-X. Li, Inorg. Chem. Commun. 14 (2011) 1422.

[16] L. T. Ghoochany, S. Farsadpour, Y. Sun, W. R. Thiel, Eur. J. Inorg. Chem. (2011) 3431.

[17] a) T. Zhou, B. Pesic, Hydrometallurgy 4 (1997) 37;

b) A. Bremer, C. M. Ruff, D. Girnt, U. Müllich, J. Rothe, P. W. Roesky, P. J. Panak, A. Karpov, T. J. J. Müller, M. A. Denecke, A. Geist, Inorg. Chem. 51 (2012) 5199.

[18] a) G. Dong, A. T. Baker, D. C. Craig, Inorg. Chim. Acta 231 (1995) 241;

b) Y. Zhou, W. Chen, Dalton Trans. (2007) 5123;

c) D. Plaul, E. T. Spielberg, W. Plass, Z. Anorg. Allg. Chem. 636 (2010) 1268;

d) G. N. Newton, T. Onuki, T. Shiga, M. Noguchi, T. Matsumoto, J. S. Mathieson, M. Nihei, M. Nakano, L. Cronin, H. Oshio, Angew. Chem. Int. Ed. 50 (2011) 4844;

e) J. S. Costa, G. A. Craig, L. A. Barrios, O. Roubeau, E. Ruiz, S. Gómez-Coca, S. J. Teat, G. Aromí, Chem. Eur. J. 17 (2011) 4960;

f) I. A. Gass, B. Moubaraki, S. K. Langley, S. R. Batten, K. S. Murray, Chem. Commun. 48 (2012) 2089.

[19] T. R. Scicluna, B. H. Fraser, N. T. Gorham, J. G. MacLellan, M. Massi, B. W. Skelton, T. G. St Pierre, R. C. Woodward, CrystEngComm 12 (2010) 3422.

[20] T. D. Roberts, F. Tuna, T. L. Malkin, C. A. Kilner, M. A. Halcrow, Chem. Sci. 3 (2012) 349.

[21] a) G. A. Craig, J. S. Costa, O. Roubeau, S. J. Teat, G. Aromí, Chem. Eur. J. 17 (2011) 3120;

b) G. A. Craig, J. S. Costa, O. Roubeau, S. J. Teat, G. Aromí, Chem. Eur. J. 18 (2012) 11703.

[22] V. A. Money, C. Carbonera, J. Elhaïk, M. A. Halcrow, J. A. K. Howard, J.-F. Létard, Chem. Eur. J. 13 (2007) 5503.

[23] Y. Lin, S. A. Lang jr., J. Heterocycl. Chem. 14 (1977) 345.

[24] G. M. Sheldrick, Acta Crystallogr. Sect. A: Found. Crystallogr. 64 (2008) 112.

[25] L. J. Barbour, J. Supramol. Chem. 1 (2001) 189.

[26] POVRAY v. 3.5, Persistence of Vision Raytracer Pty. Ltd., Williamstown, Victoria, Australia, 2002. http://www.povray.org.

[27] A. L. Spek, J. Appl. Cryst. 36 (2003) 7.

[28] C. J. O'Connor, Prog. Inorg. Chem. 29 (1982) 203.

[29] SIGMAPLOT, v. 8.02, SPSS Scientific Inc., Chicago IL (2002).

[30] a) D. F. Evans, J. Chem. Soc. (1959) 2003;

b) E. M. Schubert, J. Chem. Educ. 69 (1992) 62.

[31] W. A. Felsing, S. A. Durban, J. Am. Chem. Soc. 48 (1926) 2885.

[32] C. Kashima, S. Shibata, H. Yokoyama, T. Nishio, J. Heterocyclic Chem. 40 (2003) 773.

[33] H. Brunner, T. Scheck, Chem. Ber. 125 (1992) 701.

[34] P. van der Valk, P. G. Potvin, J. Org. Chem. 59 (1994) 1766.

[35] a) J. K. McCusker, A. L. Rheingold, D. N. Hendrickson, Inorg. Chem. 35 (1996) 2100;

b) P. Guionneau, M. Marchivie, G. Bravic, J.-F. Létard, D. Chasseau, Top. Curr. Chem. 234 (2004) 97;

c) M. Marchivie, P. Guionneau, J.-F. Létard, D. Chasseau, Acta Crystallogr. Sect. B Struct. Sci. 61 (2005) 25.

[36] J. M. Holland, J. A. McAllister, C. A. Kilner, M. Thornton-Pett, A.J. Bridgeman, M. A. Halcrow, J. Chem. Soc. Dalton Trans. (2002) 548.

[37] J. Elhaïk, D. J. Evans, C. A. Kilner, M. A. Halcrow, Dalton Trans. (2005) 1693.

[38] J. Elhaïk, C. A. Kilner M. A. Halcrow, Dalton Trans. (2006) 823.

[39] J. Elhaïk, C. A. Kilner, M. A. Halcrow, CrystEngComm 7 (2005) 151.

[40] R. Boča, Coord. Chem. Rev. 248 (2004) 757.

[41] S. A. Barrett, C. A. Kilner, M. A. Halcrow, Dalton Trans. 40 (2011) 12021.

[42] J. M. Holland, S. A. Barrett, C. A. Kilner, M. A. Halcrow, Inorg. Chem. Commun. 5 (2002) 328.

[43] J. Elhaïk, C. A. Kilner, M. A. Halcrow, CrystEngComm 7 (2005) 151.

[44] J. Elhaïk, PhD thesis, University of Leeds (2004).

Table 1. Experimental details for the single crystal structure determinations in this work.

	1[BF_4]$_2$·*x*H_2O	**1[ClO_4]$_2$**	**1[PF_6]$_2$**	**2[BF_4]$_2$**	**3[BF_4]$_2$**	**4[PF_6]$_2$**·2CH_3CN
Formula	$C_{26}H_{28}B_2F_8FeN_{10}O$	$C_{26}H_{26}Cl_2FeN_{10}O_8$	$C_{26}H_{26}F_{12}FeN_{10}P_2$	$C_{34}H_{34}B_2F_8FeN_{10}$	$C_{50}H_{42}B_2F_8FeN_{10}$	$C_{38}H_{48}F_{12}FeN_{12}P_2$
M_r	726.05	733.32	824.36	812.18	1012.41	1018.67
Crystal system	monoclinic	trigonal	monoclinic	cubic	orthorhombic	monoclinic
Space group	*C*2/*c*	*R*32	*C*2/*c*	$I\bar{4}3d$	*Pbca*	$P2_1/n$
a (Å)	17.1632(16)	18.6378(12)	34.124(3)	22.8650(18)	15.4334(17)	20.494(2)
b (Å)	20.9906(19)	–	12.3128(11)	–	14.0656(17)	23.257(3)
c (Å)	19.1771(17)	24.3461(14)	17.6817(17)	–	43.884(5)	20.609(2)
β (°)	96.605(5)	–	114.441(6)	–	–	101.271(6)
V (Å^3)	6863.0(11)	7324.0(8)	6763.4(11)	11954.0(16)	9526.3(19)	9633.3(19)
Z	8	9	8	12	8	8
T (K)	150(2)	150(2)	150(2)	150(2)	150(2)	150(2)
ρ_{calc} (g.cm^{-3})	1.405	1.496	1.619	1.354	1.412	1.405
μ (mm^{-1})	0.520	0.690	0.643	0.454	0.396	0.468
Measured reflections	37795	23056	62406	87527	162266	524427
Independent reflections	6723	4972	10895	2127	11794	23521
R_{int}	0.056	0.030	0.082	0.041	0.049	0.047
Observed reflections [$I > 2\sigma(I)$]	4552	4218	7634	1847	9529	17909
Data, restraints, parameters	6723, 40, 460	4972, 14, 216	10895, 0, 464	2127, 25, 162	11794, 0, 640	23521, 102, 1282
$R_1(I > 2\sigma(I))$[a], wR_2(all data)[b]	0.085, 0.297	0.061, 0.171	0.048, 0.132	0.048, 0.136	0.045, 0.127	0.063, 0.188

GOF	1.041	1.058	1.023	1.108	1.024	1.100
$\Delta\rho_{min}$, $\Delta\rho_{max}$ (e.Å^{-3})	–0.58, 1.05	–0.55, 0.68	–0.62, 0.78	–0.21, 0.36	–0.76, 1.00	–0.74, 0.94
Flack parameter	–	0.00(3)	–	–0.02(3)	–	–

[a] $R = \Sigma\,[\,|F_o| - |F_c|\,] / \Sigma\,|F_o|$ [b] $wR = [\Sigma w(F_o^2 - F_c^2)^2 / \Sigma w F_o^4]^{1/2}$

Table 2. Selected bond distances and angles for the crystal structures of $[Fe(L^{Me})_2]^{2+}$ (**1**$^{2+}$) salts (Å, º). α, Σ and Θ are indices showing the spin state of the complex [7,35], while θ and ϕ are measures of the angular Jahn-Teller distortion sometimes shown by $[Fe(bpp)_2]^{2+}$ centers in their high-spin state (see the text for details) [36,37]. Typical values of these parameters in $[Fe(bpp)_2]^{2+}$-type derivatives are given in ref. [7].

	1[BF$_4$]$_2$·*x*H$_2$O (Half-molecule A)	**1[BF$_4$]$_2$**·*x*H$_2$O (Half-molecule B)	**1[ClO$_4$]$_2$**	**1[PF$_6$]$_2$**
Fe−N{pyridyl}	1.958(5)	2.034(7)	2.079(6)	2.1503(16), 2.1539(19)
Fe−N{pyrazolyl}	2.019(4), 2.020(4)	2.048(6), 2.079(5)	2.140(3)–2.329(6)[a]	2.1981(17)–2.2843(17)
α	78.8(3)	77.2(2)	73.7(2)–75.0(2)[a]	74.21(14)
Σ	98.3(6)	113.7(5)	146.1(7)–153.9(7)[a]	147.8(2)
Θ	317	360	413–467[a]	456
ϕ	178.6(3)	180	178.78(16)	168.92(7)
θ	86.28(5)	89.28(5)	83.33(6)–88.13(5)[a]	78.93(2)

[a]Range of values given for all the ligand disorder sites in the molecule.

Table 3. Selected bond distances and angles for the crystal structures of salts of $[Fe(L^{All})_2]^{2+}$ (**2**$^{2+}$), $[Fe(L^{Bz})_2]^{2+}$ (**3**$^{2+}$) and $[Fe(L^{iPr})_2]^{2+}$ (**4**$^{2+}$) (Å, º). See Table 2 and refs. [7] and [35-37] for the definitions of the distortion parameters α, Σ, Θ, θ and ϕ.

	2[BF$_4$]$_2$	**3[BF$_4$]$_2$**	**4[PF$_6$]$_2$**·2CH$_3$CN (Molecule A)	**4[PF$_6$]$_2$**·2CH$_3$CN (Molecule B)
Fe−N{pyridyl}	2.129(3)	2.1357(15), 2.1436(14)	2.147(2), 2.156(2)	2.144(2), 2.145(2)
Fe−N{pyrazolyl}	2.217(3)	2.2000(15)–2.2497(15)	2.203(2)–2.255(2)	2.192(2)–2.275(2)
α	74.53(6)	74.43(12)	73.91(17)	74.08(17)
Σ	140.1(2)	141.8(2)	146.7(3)	145.7(3)
Θ	440	447	457	456
ϕ	180	171.00(6)	175.94(8)	173.50(9)
θ	90	88.11(2)	87.80(3)	89.51(3)

Table 4. Comparison of the metric parameters determining the steric influence of the methyl substituents in crystalline salts of $[Fe(L^{Me})_2]^{2+}$ (**1**$^{2+}$) and $[Fe(Me_2\text{-1-bpp})_2]^{2+}$ (Me_2-1-bpp = 2,6-*bis*{3-methylpyrazol-1-yl}pyridine). See Fig. 6 for the definitions of the parameters ***a***-***e***. All the crystal structures are of the high-spin states of the complexes, unless otherwise stated.

$[Fe(L^{Me})_2]X_2$	**X^- = BF_4^-** [a]	**ClO_4^-** [b]	**PF_6^-**
a (Fe–N)	2.019(4)-2.101(4)	2.176(3)	2.1981(17)-2.2843(17)
b (N–N)	1.367(7)-1.382(8)	1.365(4)	1.367(2)-1.377(2)
c (N–C)	1.365(11)-1.468(8)	1.458(5)	1.473(3)-1.481(3)
d (Fe–N–N)	138.1(4)-139.2(4)	138.3(2)	137.74(14)-140.26(14)
e (N–N–C)	121.2(6)-124.0(7)	120.4(3)	120.09(19)-121.52(17)
$[Fe(Me_2\text{-1-bpp})_2]X_2$	**X^- = BF_4^-** [22]	**ClO_4^-** [a] [44]	**SbF_6^-** [38]
a (Fe–N)	2.178(2)-2.204(2)	2.164(3)-2.175(3)	2.169(3)–2.214(3)
b (N–C)	1.327(4)-1.335(4)	1.319(5)-1.334(5)	1.331(5)-1.337(5)
c (C–C)	1.477(5)-1.493(5)	1.466(6)-1.494(8)	1.489(5)-1.495(5)
d (Fe–N–C)	140.1(2)-140.4(2)	140.1(3)-140.8(3)	139.7(2)-141.1(3)
e (N–C–C)	120.6(3)-121.8(3)	121.0(4)-122.8(4)	119.9(3)-121.8(4)

[a]This complex has a mixed high:low-spin state population at the temperature of measurement. [b]Only the parameters from the crystallographically ordered part of the ligand are given.

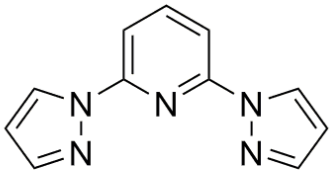

1-bpp

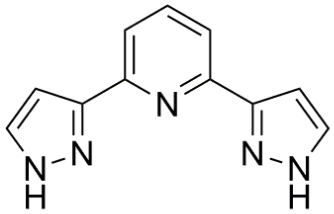

3-bpp

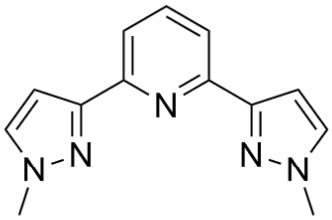

L^{Me}

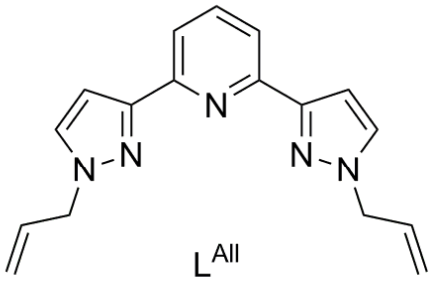

L^{All}

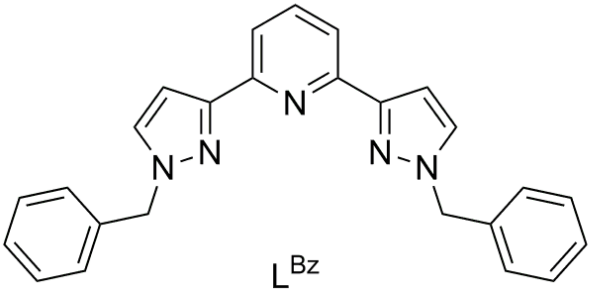

L^{Bz}

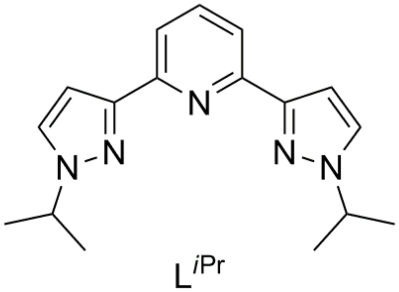

L^{iPr}

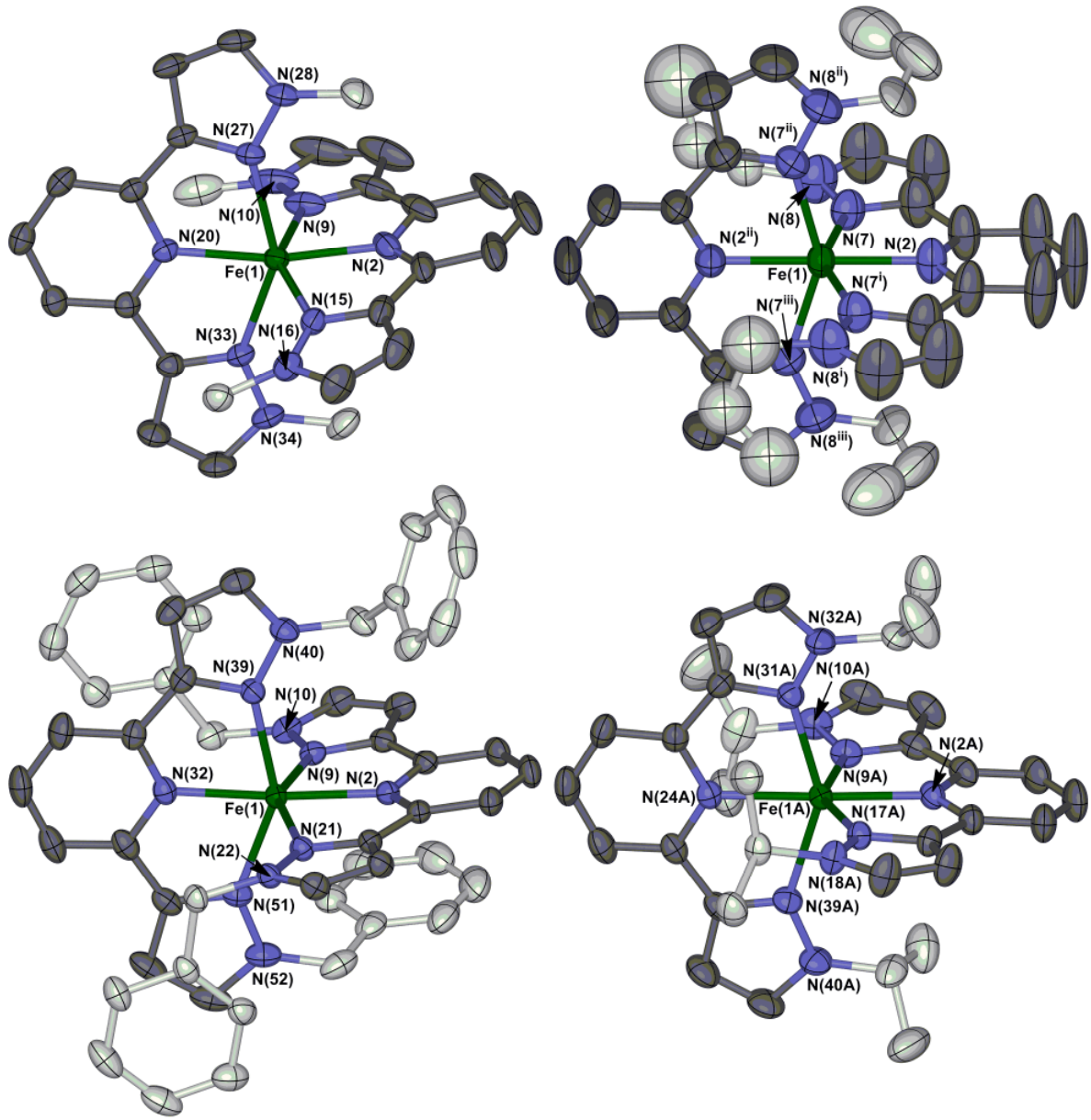

Figure 1. Views of the $[Fe(L^{Me})_2]^{2+}$ dication in **1[PF$_6$]$_2$** (top left); $[Fe(L^{All})_2]^{2+}$ in **2[BF$_4$]$_2$** (top right); $[Fe(L^{Bz})_2]^{2+}$ in **3[BF$_4$]$_2$** (bottom left); and $[Fe(L^{iPr})_2]^{2+}$ in **4[PF$_6$]$_2$**·2CH$_3$CN (molecule A, bottom right). The allyl substitutents in $[Fe(L^{All})_2]^{2+}$ are plotted in different disorder orientations, while only the major orientation of the disordered *iso*propyl group in the molecule of $[Fe(L^{iPr})_2]^{2+}$ is shown. Displacement ellipsoids are at the 50 % probability level, and H atoms have been omitted for clarity. Colour code: C (ligand backbone), dark gray; C (substituents), white; N, blue; Fe, green.

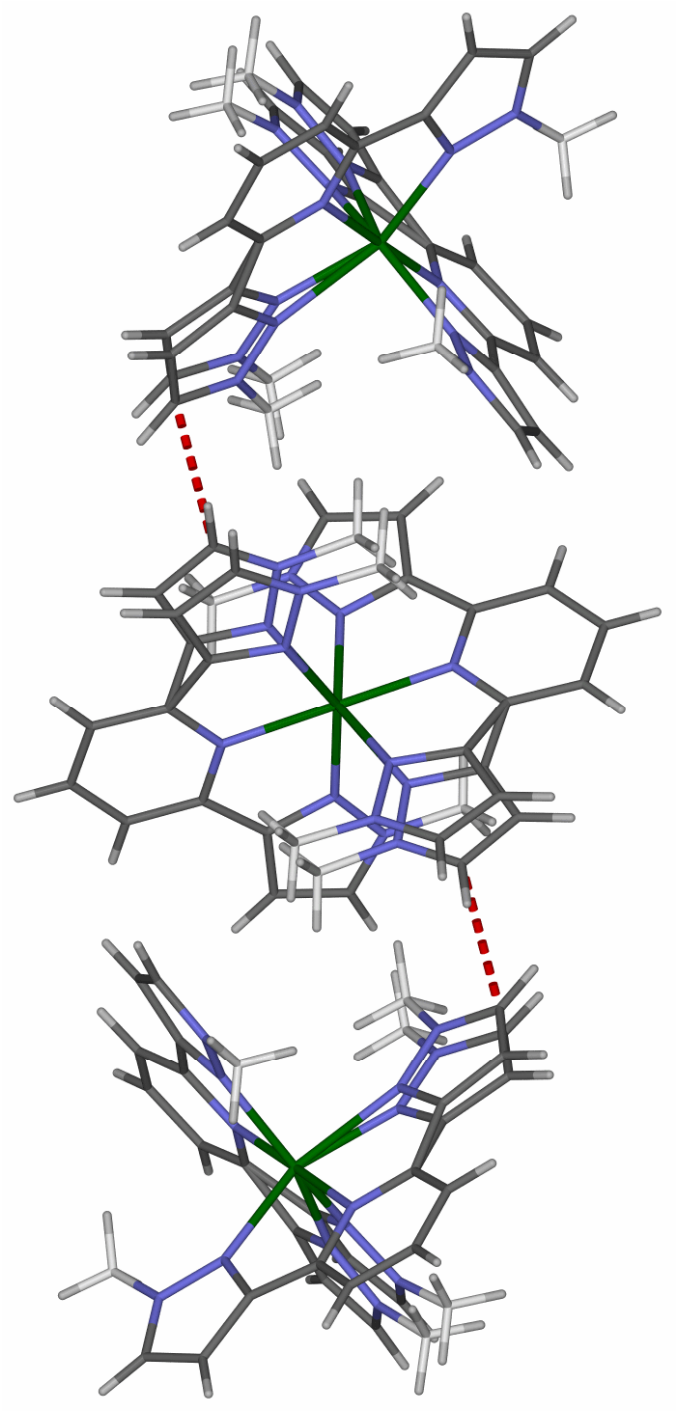

Figure 2. Partial packing diagram of **1[ClO$_4$]$_2$**, showing the intermolecular steric clash that leads to the ligand disorder. The intermolecular C…C contacts of 2.8 Å shown in red, between the 'B' disorder site on adjacent molecules related by *–x*, *–x+y*, *–z*, mean that this site cannot be simultaneously occupied in both molecules in each pair. All atoms have arbitrary radii, and the view is along the [110] vector, with the *c* axis vertical. Colour code: C (ligand backbone), dark gray; C (substituents), white; H, pale gray; N, blue; Fe, green.

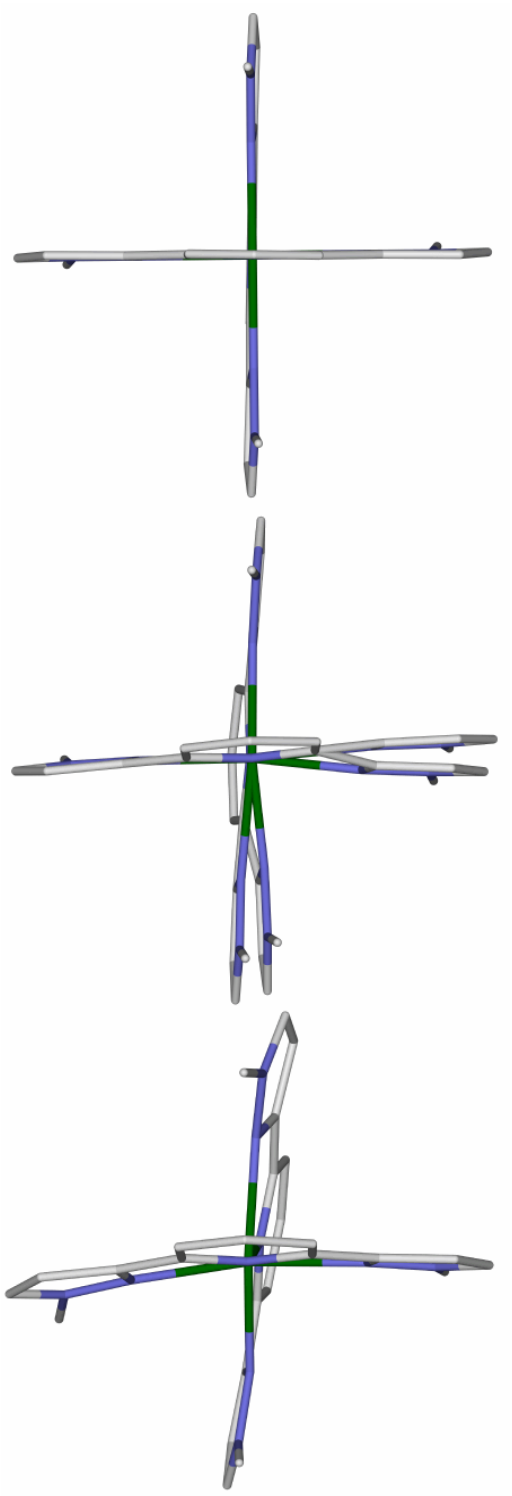

Figure 3. Comparison of the molecular structures of the $[Fe(L^{Me})_2]^{2+}$ dications in **1[BF$_4$]$_2$**·*x*H$_2$O (molecule B; top), **1[ClO$_4$]$_2$** (center) and **1[PF$_6$]$_2$** (bottom). The view in each case is along the Fe(1)–N(2) bond. All atoms have arbitrary radii, H atoms are omitted for clarity, and both disorder orientations of the L^{Me} ligand in **1[ClO$_4$]$_2$** are shown. Colour code: C, white; N, blue; Fe, green.

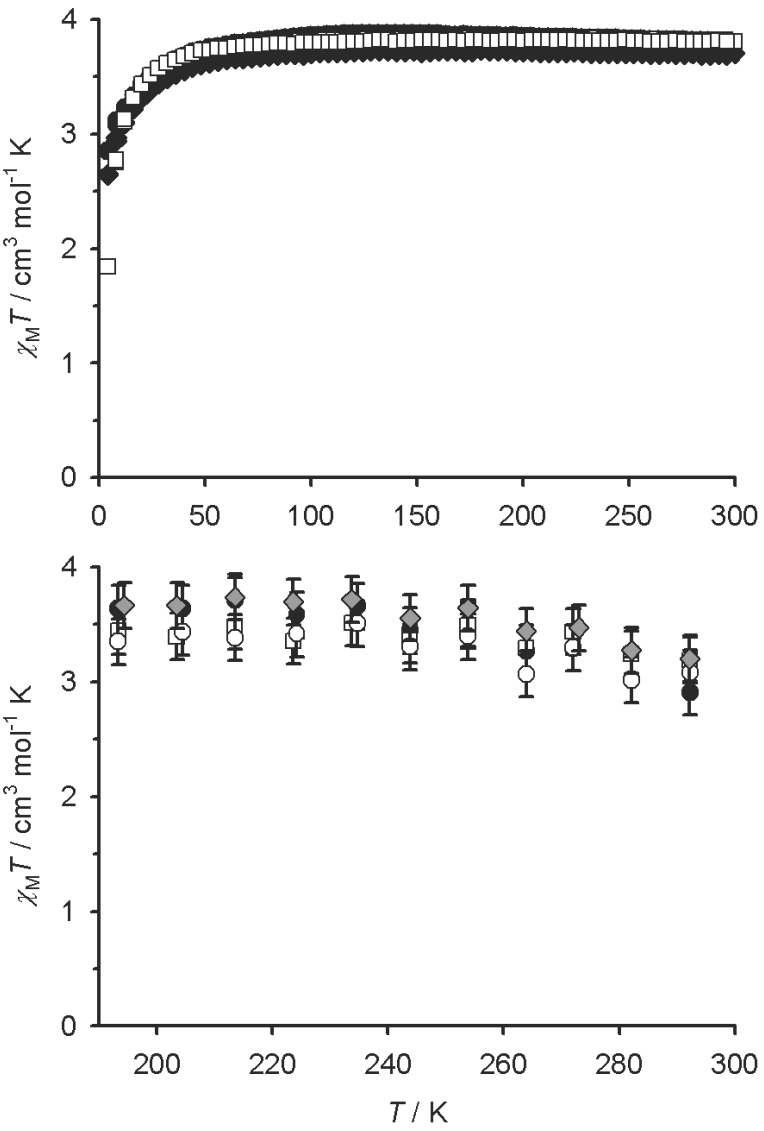

Figure 4. Top: Solid state variable temperature magnetic susceptibility data for **1[BF$_4$]$_2$** (●), **1[ClO$_4$]$_2$** (♦) and **1[PF$_6$]$_2$** (□). Variable temperature susceptibility measurements for the other complexes in this study are essentially identical to these data. Bottom: Magnetic susceptibility data in $(CD_3)_2CO$ solution for **1[BF$_4$]$_2$** (●), **2[BF$_4$]$_2$** (■), **3[BF$_4$]$_2$** (◊) and **4[BF$_4$]$_2$**·H_2O (○).

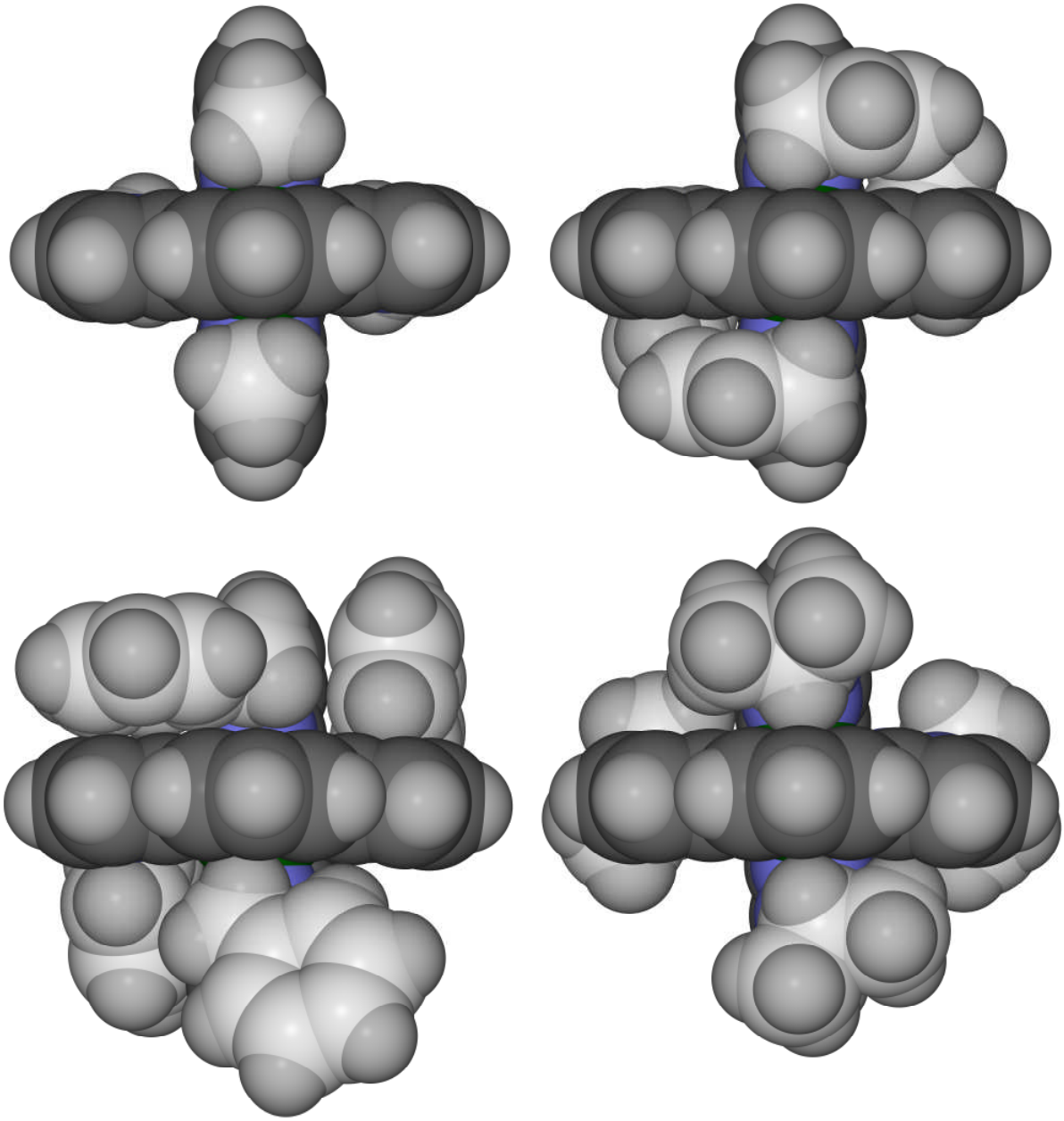

Figure 5. Space-filling views of the $[Fe(L^{Me})_2]^{2+}$ dication in **1[BF$_4$]$_2$**·*x*H_2O (molecule B; top left); $[Fe(L^{All})_2]^{2+}$ in **2[BF$_4$]$_2$** (top right); $[Fe(L^{Bz})_2]^{2+}$ in **3[BF$_4$]$_2$** (bottom left); and $[Fe(L^{iPr})_2]^{2+}$ in **4[PF$_6$]$_2$**·2CH_3CN (molecule A, bottom right). The allyl substitutents in $[Fe(L^{All})_2]^{2+}$ are plotted in different disorder orientations, while only the major orientation of the disordered *iso*propyl group in the molecule of $[Fe(L^{iPr})_2]^{2+}$ is shown. Colour code: C (ligand backbone), dark gray; C (substituents), white; H, pale gray; N, blue; Fe, green.

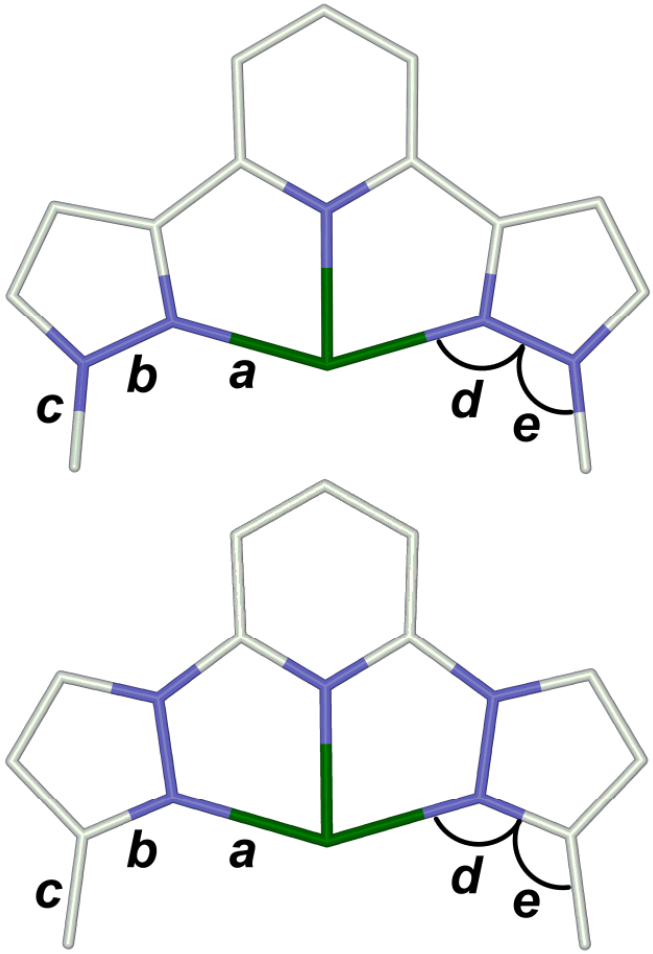

Figure 6. Comparison of the metal:ligand geometry in $[Fe(L^{Me})_2]^{2+}$ (**1**$^{2+}$, top) and $[Fe(Me_2\text{-}1\text{-}bpp)_2]^{2+}$ (bottom; Me_2-1-bpp = 2,6-*bis*{3-methylpyrazol-1-yl}pyridine). The labels ***a*-*e*** refer to the parameters listed in Table 6. Colour code: C, white; N, blue; Fe, green.